Check for updates

JGR Atmospheres

RESEARCH ARTICLE
10.1029/2021JD036231

Impacts of Lake Surface Temperature on the Summer Climate Over the Great Lakes Region

Jiali Wang[1], Pengfei Xue[1,2,3], William Pringle[1], Zhao Yang[4], and Yun Qian[4]

[1]Environmental Science Division, Argonne National Laboratory, Lemont, IL, USA, [2]Department of Civil, Environmental and Geospatial Engineering, Michigan Technological University, Houghton, MI, USA, [3]Department of Civil and Environmental Engineering, Massachusetts Institute of Technology, Cambridge, MA, USA, [4]Pacific Northwest National Laboratory, Richland, WA, USA

Key Points:

- Small differences in lake surface temperature (LST) can change summer climate at both local and nonlocal scales over the Great Lakes Region (GLR)
- Warmer LSTs create an unstable environment and enhance isolated deep convection downwind of the GLR
- The influences of the difference in LST are robust and significantly larger than the model's internal variability

Supporting Information:

Supporting Information may be found in the online version of this article.

Correspondence to:

J. Wang and Y. Qian,
jialiwang@anl.gov;
yun.qian@pnnl.gov

Citation:

Wang, J., Xue, P., Pringle, W., Yang, Z., & Qian, Y. (2022). Impacts of lake surface temperature on the summer climate over the Great Lakes Region. *Journal of Geophysical Research: Atmospheres*, *127*, e2021JD036231. https://doi.org/10.1029/2021JD036231

Received 18 NOV 2021
Accepted 13 MAY 2022

Author Contributions:

Conceptualization: Jiali Wang, Pengfei Xue, Yun Qian
Formal analysis: Jiali Wang, William Pringle, Zhao Yang
Investigation: Jiali Wang, Zhao Yang
Methodology: Jiali Wang, Pengfei Xue, Yun Qian
Resources: Jiali Wang
Supervision: Pengfei Xue, Yun Qian
Validation: Jiali Wang, William Pringle
Visualization: Jiali Wang, William Pringle
Writing – original draft: Jiali Wang
Writing – review & editing: Pengfei Xue, William Pringle, Zhao Yang, Yun Qian

© 2022. American Geophysical Union. All Rights Reserved.

Abstract The surface of the Great Lakes interacts with the atmosphere, influencing the weather and climate over the Great Lakes Region (GLR). However, most climate models were not designed with sufficient emphasis on lake–atmosphere interactions, which could potentially cause model biases over the GLR. To understand how lake surface temperature (LST) affects the regional summer climate over the GLR, we conducted twin experiments using the Weather Research and Forecasting model at a spatial resolution of 4 km using two different LST data sets as the bottom boundary condition over the Great Lakes. Our simulations include 10 ensemble members for the summer of 2018 and a single multiyear run for the summers of 2014–2020. Results show that variations in LST influence atmospheric temperature and moisture at a local scale—while affecting the convective environment and precipitation processes over a much larger spatial scale. In particular, an LST that is only 1°C–3°C warmer (depending on the lake) increases near-surface air temperature by 1.93°C and 0.97°C over Lake Superior and Lake Erie, respectively, and increases evaporation over the lakes by 0.23 and 1.1 mm day^{-1}. The warmer LST reduces mesoscale convective precipitation upstream of the GLR; however, it increases isolated deep convective precipitation and nonconvective precipitation downstream of GLR due to increased local instability and enhancement of moisture transport. Our analyses confirm the robustness of these impacts, which is at least 2 times larger than the model internal variability and is seen across all simulated summer seasons.

1. Introduction

The total surface area of the Great Lakes is over 94,250 miles^2. Consisting of five large lakes, they contain over one fifth of the world's total surface fresh water, with depths of up to 400 m (EPA, 2020). The Great Lakes substantially influence the regional weather and climate via their effects on the atmospheric energy and water budget; open water typically has greater thermal conductance, lower albedo, and lower roughness compared to soil or vegetated surfaces (Notaro et al.,2013; Scott & Huff, 1996). The large thermal inertia of the lakes leads to a reduction in annual and diurnal temperature ranges across the Great Lakes Basin (Harris & Kotamarthi, 2005; Notaro et al., 2013). Mean minimum temperatures in the region are warmer during all seasons and over all five lakes, while maximum temperatures are cooler during spring and summer (Scott & Huff, 1996).

Lake thermal impacts and associated evaporation have a strong influence on regional precipitation patterns. While many studies have investigated the impact of lake surface temperature (LST) on the cold-season precipitation—which is primarily a direct product of warmth and moisture from the Great Lakes (e.g., lake-effect snow; Notaro et al., 2021; Shi & Xue, 2019)—the impact of LST on summer precipitation has only rarely been studied. During early summer, the lake surface is still relatively cool compared to the atmosphere, resulting in condensation on the lake surface and a stable boundary layer that deters over-lake convective processes (Miner & Fritsch, 1997; Workoff et al., 2012). Due to the temperature differences over lake and inland, lake breeze can cause air to rise inland and increases the likelihood of over-land precipitation (Schulkowski, 2020). During late summer, while the land cools and the lakes remain warm, the temperature differential between land and lake surface coupled with baroclinic waves (e.g., cold front and trough) and/or the Great Plains low-level jets can generate enhanced precipitation (Feng et al., 2016; Miner & Fritsch, 1997). Therefore, changes in summer LST could potentially affect its feedback to atmospheric stability and change the water and energy budget over the entire Great Lakes Region (GLR). The summer is an ideal time to evaluate the influence of LST on the lake surface–atmosphere

feedbacks, because the convective environment is highly dependent upon local instability in the summer, and sufficient surface observations are available on both land and lakes for model evaluation.

Furthermore, in the past few decades changes have been detected in the climate over the GLR. For example, observational analyses suggest that extreme summertime precipitation has increased (Kunkel et al., 2003, 2012) over the GLR over the past 30 years. Much of this increase is associated with convective systems that dominate warm season extreme precipitation in the region (Feng et al., 2016; Workoff et al., 2012), leading to deadly and destructive flash flooding (Hu et al., 2020; Schumacher & Rasmussen, 2020). These changes to the GLR climate are thought to be caused by the warming of LST in summer and the decline of winter ice cover under the influence of global warming (Austin & Colman, 2007).

Therefore, it is important to better understand the GLR climate and its changes going forward. However, most general circulation models (GCMs) do not even include the Great Lakes as a modeled surface element, and those that do include the lakes do not incorporate a dynamic coupling between the lakes and the atmosphere. Because the spatial resolution of GCMs is coarse (e.g., 100–300 km), the Great Lakes are either geometrically ignored or treated as a water surface without much consideration to the accuracy of the LST (Delaney & Milner, 2019; Xiao et al., 2018). This can cause substantial model bias over the GLR—or over an even greater area—and regional climate models (RCMs) could also inherit this bias when they use GCMs as forcing data for dynamical downscaling. In RCMs, if the lakes are not resolved in the forcing data—especially if the lakes are geographically distant from resolved water bodies—a "search" option is employed to extrapolate LST from the closest water point with valid data (Spero et al.,2016; Xiao et al., 2018). For the Great Lakes, this means that the LSTs can come from the sea surface temperature (SST) of Hudson Bay and the Atlantic Ocean. This situation can cause the LST values to be either unrealistically too warm or too cold. For example, RCM studies using the Community Earth System Model (CESM) output for lateral boundary conditions found that extrapolation methods create nonphysical discontinuities where the temperatures are extrapolated from different bodies of water (Mallard et al., 2015; Spero et al., 2016). These discontinuities not only cause model biases near the lakes but also affect predicted extremes hundreds of kilometers from the lakes (Spero et al., 2016).

The need for more comprehensive coupled land–lake–atmosphere RCMs to address these deficiencies has been stressed before (Sharma et al., 2018). In the Coordinated Regional Climate Downscaling Experiment—North American project, some RCMs (e.g., Canadian regional climate model, Scinocca et al., 2016) couple with a one-dimensional lake model called the Fresh Water Lake model (Mironov et al., 2004), which can provide improved results compared to the interpolation approach (Gula & Peltier, 2012; Xiao et al., 2018). Other researchers have developed more complex coupled modeling systems using three-dimensional hydrodynamic lake models that were shown to be even more accurate than the RCMs with one-dimensional lake models (Sun et al., 2020; Xue et al., 2017).

Nevertheless, the effects of Great Lakes surface temperature on the GLR summer climate have not been fully investigated. Spero et al. (2016) demonstrated such impacts on daily maximum temperature and sea level pressure in July and December based on 3 years of simulation at a spatial resolution of 36 km, using CESM and the lake model within the Community Land Model as two different LST data sources for bottom boundary conditions in an RCM. A more complete assessment of LST impacts on summer climate and precipitation remains unclear. Providing this information would help contextualize previous studies that did not consider atmosphere–lake interactions when projecting the future climate over the GLR (e.g., Christensen et al., 2007; Mearns et al., 2009; Wang & Kotamarthi, 2015).

The goal of our study is to understand how different LST data sets can potentially influence atmospheric simulations over the larger GLR during the summer (June–August) in an RCM, focusing on how convective processes and precipitation are affected. To this end, we conduct a historical reanalysis of the years 2014–2020 (with 10 ensemble members for 2018) using different observational LST data sets for the Great Lakes. To evaluate the relative importance of these impacts, we compare them with model internal variability caused by model nonlinearity and interannual variability caused by large-scale oscillations. By taking advantage of the recently developed state-of-the-art tracking algorithm for rainstorms (Feng et al., 2019; Li et al., 2021), we are able to distinguish the precipitation caused by mesoscale convective systems (MCSs), isolated deep convections (IDCs), and nonconvections. We show that if there are some errors in LST, it can affect evaporation and precipitable water (PW) at a local scale; moreover, it can affect moisture flux transport and convective available potential energy over a much

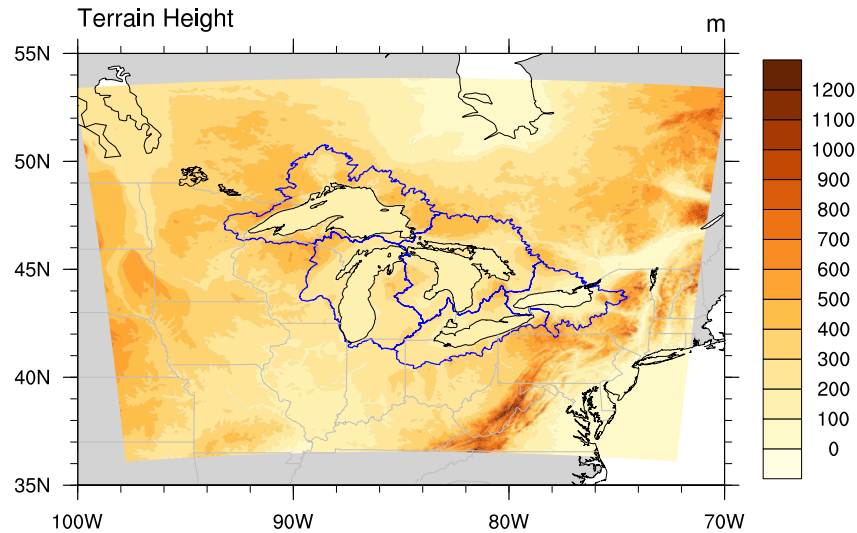

Figure 1. Weather Research and Forecasting (WRF) model domain with terrain height in meters. We refer to this entire research domain as the Great Lakes Region (GLR). The Great Lakes Hydrological Basin (GLHB) is outlined in blue.

larger spatial scale. Consequently, the MCS-induced precipitation is decreased upstream of Great Lakes Basin, while IDC-induced precipitation is increased downstream of Great Lakes Basin. Understanding these impacts is important for both short- and long-term lake level predictions as well as weather predictions of convections near the lakes.

2. Model, Data, and Approach

2.1. RCM Configuration and Experimental Design

The RCM used in our modeling experiments is based on the Weather Research and Forecasting (WRF) model version 4.2.2 with the Advanced Research WRF dynamic core (Skamarock & Klemp, 2008). The model domain is centered at 45.5°N and 85.0°W and has dimensions of 544 × 485 grid points in the west–east and south–north. Grid spacing is 4 km, covering the GLR as shown in Figure 1 with the Great Lake Hydrological Basin (GLHB) outlined. There are 50 stretched vertical levels topped at 50 hPa. The initial and boundary conditions are constructed from 3-hourly 0.25° European Centre for Medium-Range Weather Forecasts atmospheric reanalysis of the global climate, version 5 (ERA5; Bell et al., 2020). The WRF model incorporated Thompson microphysics (Thompson et al., 2004, 2008), the Rapid Radiative Transfer Model for GCMs longwave and shortwave schemes (Iacono et al., 2008), the Yonsei University planetary boundary layer scheme (Hong & Lim, 2006; Noh et al., 2003) and revised Atmospheric Research Mesoscale Model Monin–Obukhov surface layer scheme (Jiménez et al., 2012), and Unified Noah land surface model (Chen & Dudhia, 2001). No subgrid cloud cover or shallow cumulus parameterizations are used. No boundary nudging is applied, so the model can develop its own variability (e.g., spatial and internal variability) across the region.

To explore the impacts of different LST data sets, we performed a set of twin experiments. In the first experiment, the WRF model used SST data from ERA5 (ELST hereafter, see data description in Section 2.3) as its lower boundary condition over the Great Lakes. We refer to this experiment as WRF_ELST hereafter. Note that in WRF by default, no mask is applied for the SST data. This was a problem for the ERA5 SST downloaded from the Copernicus website, which caused missing SST values along the land–water interface. This is a particular issue for the GLR along the lake boundaries which can create nonnegligible bias in air temperature, evaporation, moisture, and wind largely over the lakes and the GLHB (see Supporting Information S1). In this study, we applied a land/water mask for the SST in the METGRID.TBL during preprocessing of WRF and fixed the issue in SST values along the land–water interface. The configuration of the second experiment was the same as the first experiment, except that the LSTs over the Great Lakes were replaced with a National Oceanic and Atmospheric Administration (NOAA) Great Lakes Surface Environmental Analysis (GLSEA) data set (Schwab et al., 1992;

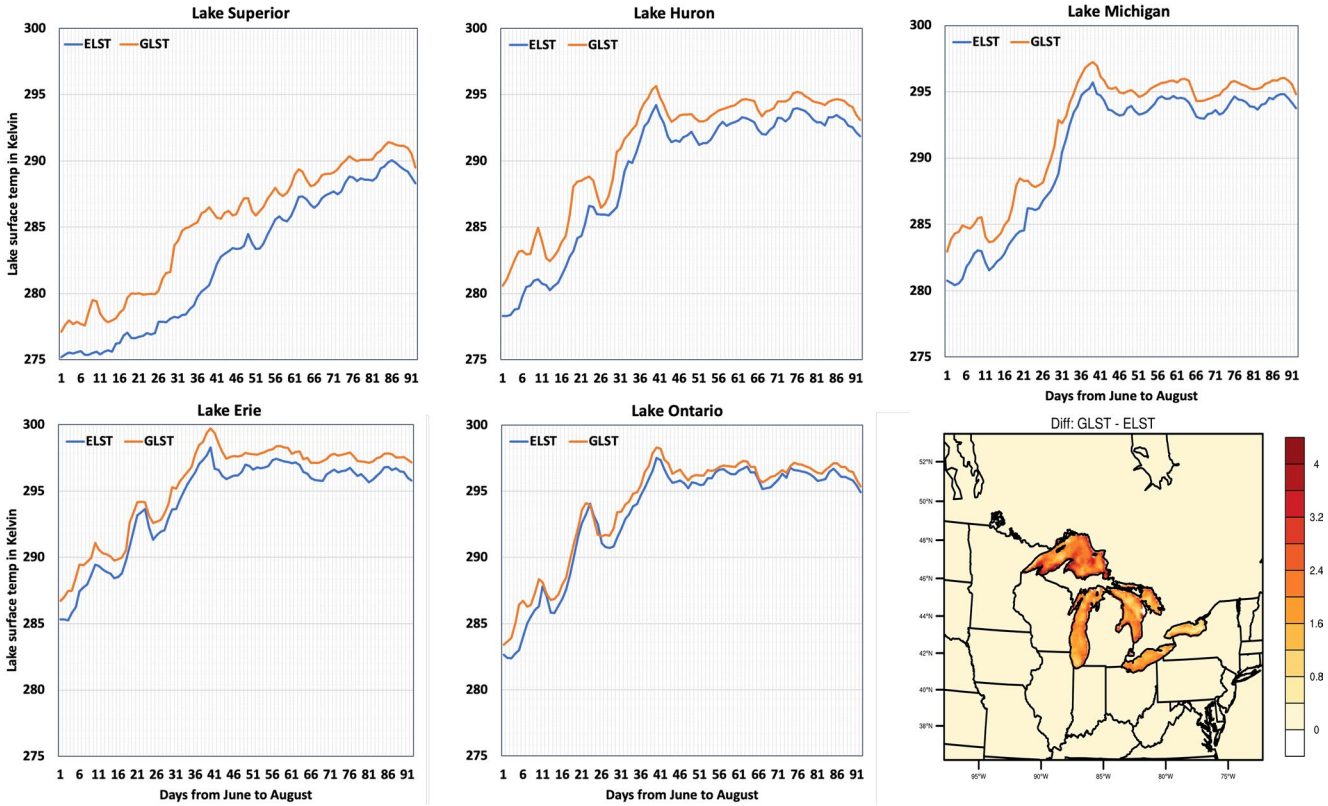

Figure 2. Daily lake surface temperature (LST) from ERA5 ("ELST") and Great Lakes Surface Environmental Analysis ("GLST") averaged over the five lakes from June to August in 2018. Other years show similar LST differences between the two data sources. Lower right: LST difference between GLST and ELST across the entire GLR.

GLST hereafter, see Section 2.3 for more information). We refer to this experiment as WRF_GLST hereafter. The SSTs for water points over the Atlantic Ocean are the same for both experiments.

Figure 2 shows the five lake-averaged summer (June–August) GLST and ELST, and the summer mean difference between GLST and ELST across the model domain (GLR hereafter). Overall, Lake Superior is the coolest and Lake Erie is the warmest. GLST is warmer than the ELST over all five lakes. Over Lake Superior, GLST is higher than ELST by 2.7°C averaged across the lake from June to August, with the largest difference being 6.5°C in late June and early July. Over Lake Huron and Lake Michigan, the lake-average difference from June to August is 1.94°C and 1.8°C, respectively. The differences between GLST and ELST over Lake Erie and Ontario are smaller compared to other lakes: 1.27°C and 0.76°C, respectively. More importantly, the high-resolution (1.3 km) GLST data accurately represented the spatial pattern of the LST, including the warmer coastal waters and relatively cold offshore waters, especially those in the southern lakes in late spring and early summer (e.g., southern Lake Michigan, Lake Erie, and Lake Ontario; see Figure 3). Such spatial patterns are clearly missing in the relatively coarse-resolution ELST data, which may cause additional biases when these patterns are used as over-lake boundary conditions in WRF simulations. Hence, ELST is intended to represent the relatively biased LSTs used as boundary conditions for many large-scale models, whereas GLST is a more realistic data set based on high-resolution remotely sensed products. The experiment then evaluates the sensitivity of the RCM to the differences in the two LST products.

While Figures 2 and 3 show an example from summer 2018, the same spatiotemporal patterns are seen in the other years analyzed (2014–2020) as well. The warmer GLST can potentially influence the water and energy budget over the GLR. Even for Lake Erie and Lake Ontario, where the differences in LST are small, the GLST warming effects on the atmosphere over these two lakes could be complicated, because (a) they are downwind of the GLR, which shows the largest response from the lake effect (Notaro et al., 2013; Scott & Huff, 1996) and (b) there is a rise in elevation east of Lake Erie and Lake Ontario.

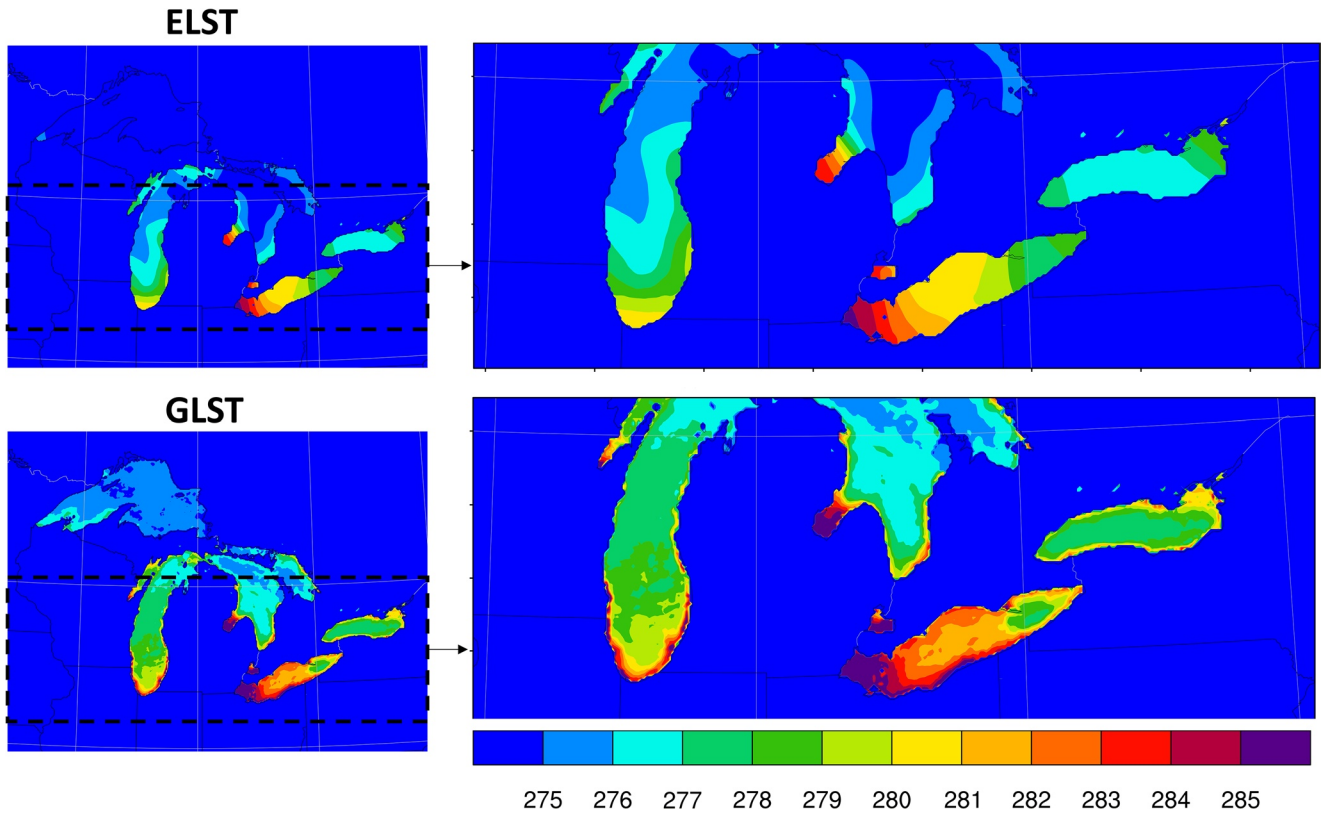

Figure 3. ELST (top row) and GLST (bottom row) on 12 May 2018, both derived from the lower boundary conditions of WRF (namely wrflowinp_d01) at a spatial resolution of 4 km. ELST is based on a spatial resolution of 0.25° (~27.5 km), and GLST is based on a spatial resolution of 1.3 km.

We conducted 10 ensemble members for each of the twin experiments in 2018, generating the model simulations from different hours of a day or different days of a month. The 10 members started with initial conditions 12 hr apart between 0000 UTC on 12 May 2018 and 1200 UTC on 16 May 2018; they ended on 0000 UTC 1 September 2018. Therefore, the 10 members overlapped for the entire summer of 2018, with a spin-up period varying from 15 to 19 days. We also conducted one-member simulations for both experiments (WRF_GLST and WRF_ESLT) for a longer period from 2014 to 2020 (pre-2014 data sets have significant bias, see description in Section 2.2). The total 7-year one-member run provides more data, which allows for more robust statistical analysis (e.g., investigating the interannual variabilities and calculating the upper percentiles of different quantities). The 7-year run started on 0000 UTC on 12 May and ended on 0000 UTC 1 September of each year. The resulting simulations were all analyzed starting 1 June 2018 after a spin-up period ranging from 15 to 19 days (depending on the starting point for each ensemble member).

2.2. Data

The SST data used in ERA5 come from two external providers. Before September 2007, SST from the Met Office Hadley Center's SST version 2 data set was used, which is a combination of monthly globally complete fields of SST and sea ice concentration on a 1° latitude–longitude grid from 1850 to the present. From September 2007 onward, the Operational SST and Ice Analysis data were used, which are a high-resolution (~5 km) daily SST operationally produced at the UK Met Office (Donlon et al., 2012), with various types of instruments analyzed together. In the pre-2014 ERA5 SSTs of the Great Lakes, there are significant cold biases in winter and a warm bias in summer due to model errors and unrealistically high temporal variabilities (Simmons et al., 2021). Therefore, for a fair comparison, we only conducted simulations for the 2014–2020 period when ERA5 SST is reliable. The NOAA GLSEA provides daily digital maps of the Great Lakes LSTs stored as 1,024 × 1,024-pixel maps with a horizontal spatial resolution of ~1.3 km. The GLSTs are derived from Advanced Very High-Resolution Radiometer onboard polar-orbiting satellites, with an observation frequency of 2–3 times per day. The LST

information was updated daily using the cloud-free portions of the satellite imagery. We studied the summer months here because this data set is more accurate in summer, without too much interruption from clouds, unlike the winter season. Comparing the time series of ELST and GLST since 2014, we found ELST is systematically lower than the GLST, as shown in Figure 2, which provides a good opportunity to explore the impacts of a consistent difference in the LSTs.

In situ NOAA National Data Buoy Center (NDBC) buoy observation data were used to evaluate LST, near-surface air temperature, and winds and estimated heat fluxes of ERA5, WRF-ELST, and WRF-GLST at nine selected sites (shown in Figure 5) over the five lakes. NDBC provides hourly measurements of LST, air pressure, wind velocity, and air and dewpoint temperature at arbitrary heights. We used Monin–Obukhov theory with coefficients and equations from Laird and Kristovich (2002), with modification of the Charnock coefficient to 0.0185 to match that used in WRF, to compute wind and air temperature at standard heights (10 and 2 m, respectively), as well as sensible and latent heat fluxes. Note that the dewpoint temperature needed for the latent heat flux estimate was more scarcely observed (5%–92% of the time depending on the buoy) than other quantities resulting in a more limited time series.

2.3. Metrics for Model Validation

To evaluate the model performance and potential changes when different SSTs were used as the lower boundary conditions in the WRF simulations, we compared the output from the twin experiments (WRF_ELST and WRF_GLST) with observations over the Great Lakes and the surrounding land. We assessed the model performance in seasonal mean, diurnal patterns, and extremes, such as 95th percentiles of hourly near-surface (2-m) air temperature, near-surface (10-m) wind speed and direction, precipitation, sensible heat flux, and latent heat flux. The model evaluations were conducted using the 7-year model output at hourly interval from 2014 to 2020. To examine the impact of a different LST on the atmosphere, we compared the twin experiments regarding the variables that can potentially influence the water and heat budget in the atmosphere. The variables include 2-m air temperature, evaporation calculated from latent heat flux, PW, integrated water vapor transport (IVT; Lavers & Villarini, 2013), and the maximum convective available potential energy (MCAPE) computed by lifting the air parcel with the maximum equivalent potential temperature found in the first 3 km; lifting condensation level (LCL), which is a useful proxy for the moisture deficit in the lower atmosphere that could inhibit convection (Lahmers et al., 2020; Santanello et al., 2018); and the amount of various types of precipitation (see description in Section 2.4). The analyses were conducted using both 2018 ensemble simulations and 7-year (2014–2020) simulations.

2.4. Tracking Algorithm for Different Types of Precipitation

Precipitation generated by MCSs and IDCs showed a clear seasonal pattern; over the central and east portion of the continental United States (Li et al., 2021), including the GLR, the amount nearly doubled during the spring and summer (~100 mm) compared to the autumn and winter (~56 mm). Therefore, it is important to investigate summer storms and to understand how LST affects the different types of summer storms over GLR. In this study, instead of looking at the overall precipitation change as in previous studies (e.g., Liu et al., 2017; Zobel et al., 2018), we used the Flexible Object Tracker (FLEXTRKR) algorithm developed by Feng et al. (2018, 2019) and enhanced by Li et al. (2021), to distinguish MCSs, IDC, and nonconvective precipitation based on their unique spatiotemporal convective characteristics.

Many tracking algorithms focus on the change of storms' characteristics and morphology, such as intensity, size, and duration (e.g., Chang et al., 2016; Prein et al., 2020; Workoff et al., 2012); however, most tracking algorithms only examine the horizontal dimensions and cannot distinguish between the MCS and the IDC. In contrast, the FLEXTRKR algorithm can identify the three-dimensional structure of convective systems and has shown its applicability using both observation-based data and model simulations (Li et al., 2021). By tracking the MCS and IDC in the twin experiments, we focused on changes in the amount of precipitation from MCS, IDC, and nonconvective precipitation.

2.5. Model Internal Variability Evaluation

A model's internal variability could be large due to the nonlinearity of the WRF model when the model simulation is at a higher spatial resolution. For example, the internal variability for a simulation with 12-km resolution is twice as large as that for a simulation with 50-km resolution in the summer over the central and eastern United States (Wang et al., 2018). The internal variability is especially important during the summer over the GLR, because part of the summer precipitation is driven by local convective processes that are much more prone to triggering internal variability within the RCM. To evaluate the relative importance of the impacts of a different LST, we assessed the internal variability in our twin experiments at a grid spacing of 4 km. Internal variability was quantified using the standard deviation of the 10 ensemble members of the variables of interest (see details in Wang et al., 2018). The internal variability is especially important during summer over the GLR, because the internal model variability related factors such as random and nonlinear behavior in the convection and precipitation process as well as associated local land–atmosphere interactions are maximum in summer, while in winter stronger westerly flow can sweep away much of the internal generated model response.

2.6. Statistical Verifications

Because we evaluated LST impacts on a seasonal scale, we conducted statistical verifications at the same scale in order to understand the relative importance of the LST impacts compared with internal variability and interannual variability. To compare internal variability versus LST impacts on the atmosphere, we first calculated the seasonal average of each ensemble member and then the standard deviation of the 10 members. The internal variability at seasonal scale was considered as noise relative to the impacts from a different LST on the 10 ensemble simulations, which were also quantified using a seasonal mean. If the impact on a certain atmospheric variable was more than twice the noise caused by the internal variability, then the difference between the twin experiments (WRF_GLST vs. WRF_ELST) for that variable was considered statistically significant at the 95% confidence level by assuming the seasonal-averaged variables on (or close to) a Gaussian distribution.

For interannual variability, we tested the significance of the difference between the two experiments for the 7-year simulations using a Student's *t*-test, with a *p*-value smaller than 0.05 indicating a 95% confidence level. We did not use signal-to-noise ratio to compare the LST impacts versus the interannual variability, because the interannual variability of the 7-year data was expected to be much larger than the impacts caused by a different LST.

3. Results

3.1. Impacts of Great Lakes Surface Temperature on Local Atmosphere

Compared to in situ LST observations at the NDBC lake buoys throughout June–August 2014–2020, both ELST and GLST data sets had a systematic bias of similar magnitude, but of opposite sign (Figure 4). The ELST was found to have a mean cold bias of 0.68°C ± 0.39°C (value after the ± indicates the standard deviation), while the GLST had a mean warm bias of 0.70°C ± 0.30°C at nine locations (Figure 5). The root-mean square errors of both LST sources were also comparable (∼1.5°C on average). Note that the in situ LST observations are the measured lake temperature at depths of ∼1 m and therefore have some bias of their own compared to the skin temperature of the lake (Liu et al., 1979). Based on our own three-dimensional lake simulations (Xue et al., 2017), we estimated that on average the lake temperature at the surface is 0.26°C ± 0.13°C warmer than that at the buoy-measured depths during the summer months. Hence, it is likely that the warm bias of GLST is smaller and the cold bias of the ELST is greater than the values quoted above by about a quarter of a degree (Celsius). In any case, rather than focus on the accuracy of the two LST data sources, we instead highlighted the systematic discrepancy (∼1.4°C) between the warmer GLST and the colder ELST (Figure 2), and the resultant effects of this LST difference on the atmosphere and climate (Section 3.2). As mentioned earlier, GLST can capture finer spatial variabilities (e.g., warmer coastal waters and the relatively colder waters offshore) due to its higher spatial resolution, which can potentially affect the model solution for the lakeshore (e.g., lake breeze, urban heat island) and even regions far away from the shoreline (see Section 4).

Figure 5 shows the statistical distribution of T2 from buoy observations, ERA5 data, WRF_ELST output, and WRF_GLST output at the NDBC buoy locations throughout June–August 2014–2020. In general, both ERA5 reanalysis and the WRF simulations captured the spatial variability of air temperature across all five lakes. ERA5

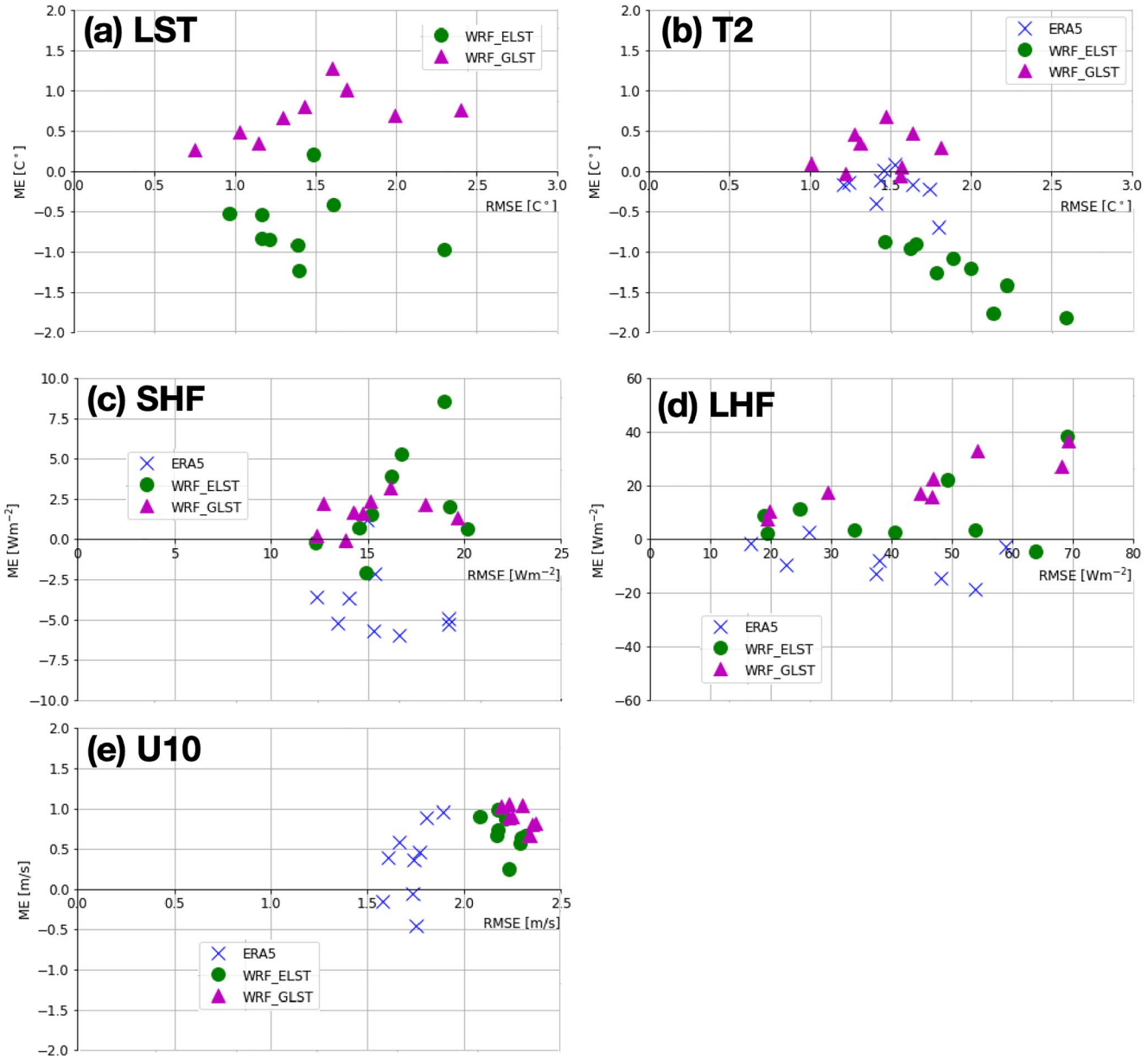

Figure 4. June–August 2014–2020 mean error (ME) versus root-mean square error (RMSE) scatter plots at nine in situ National Data Buoy Center (NDBC) observations (locations shown in Figure 5) for the ERA5 reanalysis data and the WRF models: (a) lake surface temperature (LST), (b) 2-m air temperature (T2), (c) sensible heat flux (SHF), (d) latent heat flux (LHF), and (e) 10-m wind speed (U10) calculated by zonal and meridional winds.

showed an air temperature similar to buoy observations with a mean bias of −0.20°C ± 0.22°C. WRF_ELST underestimated the air temperature over all lakes in both the mean (−1.3°C ± 0.33°C) and the extremes (the overall distribution is shifted colder). WRF_GLST did not suffer from this cold bias; instead, it matched closer to the buoy observations and ERA5, with a mean bias of +0.25°C ± 0.24°C (Figures 4b and 5). These results indicated the importance of high-resolution and more accurate LST information for over-lake boundary conditions for the simulation of air temperature. The sensible heat fluxes at the NDBC buoys in WRF_GLST also had a smaller mean bias (0.67 ± 1.3 W m^{-2}) and standard deviation than both WRF_ELST (1.3 ± 3.4 W m^{-2}) and ERA5 (−4.9 ± 2.2 W m^{-2}) compared to buoy measurements (Figure 4c). The reduction in bias of both T2 and the sensible heat fluxes by using the warmer GLST was found to be statistically significant (*t* test) at all buoy locations except for 45006 for the heat flux. On the other hand, both WRF models overestimate latent heat fluxes and

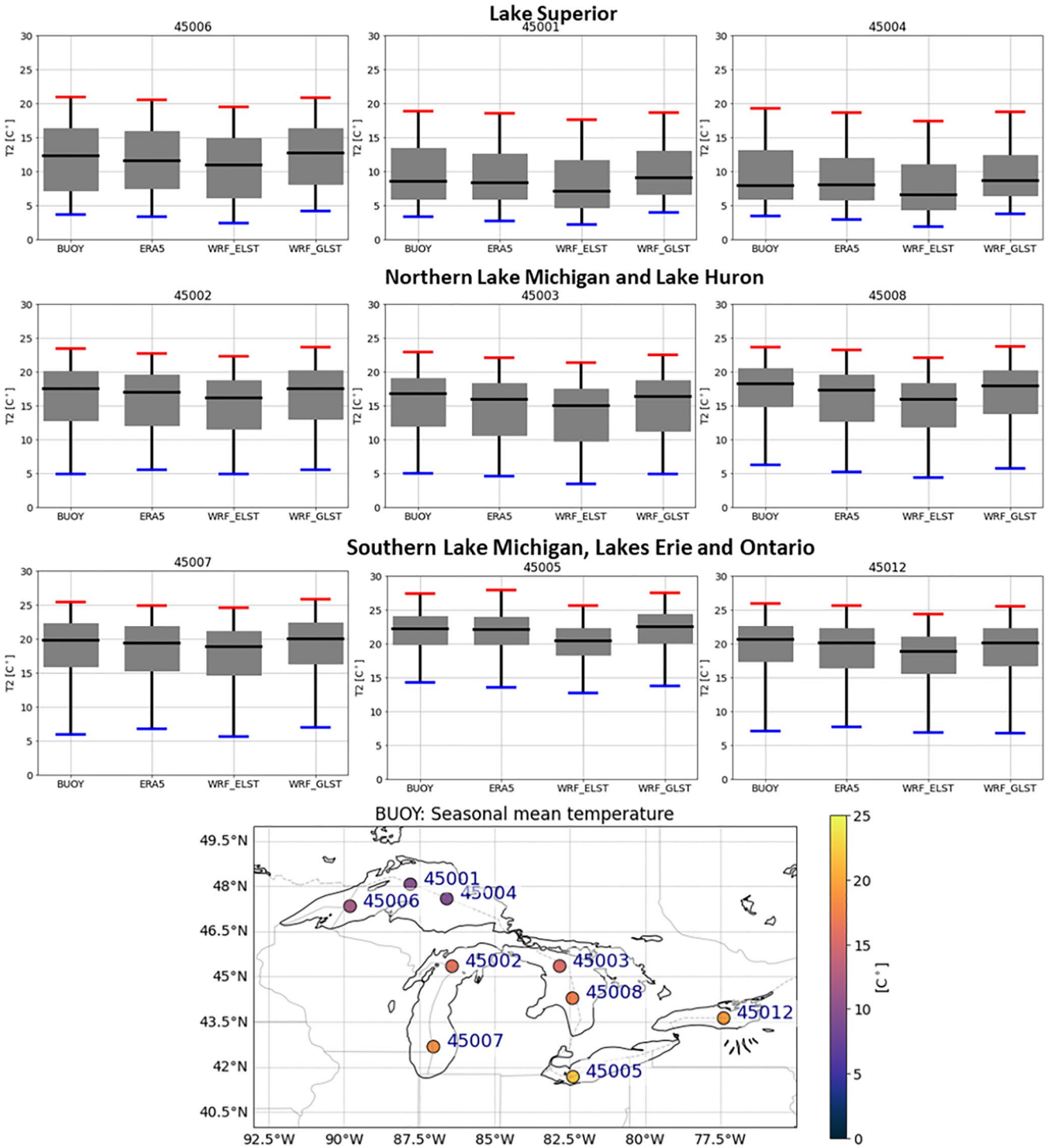

Figure 5. Geographic locations and seasonal mean 2-m air temperature (T2) of NDBC lake buoys (bottom) and T2 distributions (box plots) during 2014–2020 June–August, comparing in situ observations, ERA5 reanalysis data, WRF_ELST, and WRF_GLST. The box plots were created based on hourly T2 over the 7 years. Black lines: median. Box edges: 25th and 75th percentiles. Whiskers: 1st and 99th percentiles. Lake Superior refers to buoys 45001, 45004, and 45006; Northern Lake Michigan and Lake Huron refer to buoys 45002, 45003, and 45008; and Southern Lake Michigan, Lake Erie, and Lake Ontario refer to buoys 45007, 45005, and 45012.

10-m wind speeds and the mean biases were greater in the WRF_GLST (21 ± 9.2 W m^{-2}, 0.84 ± 0.14 m s^{-1}) than WRF_ELST (9.6 ± 12 W m^{-2}, 0.66 ± 0.21 m s^{-1}; Figure 4e). This may indicate that the lake surface boundary layer scheme in the WRF model needs adjusting as these were developed for the open ocean, similar to suggestions for shallow ocean waters (Jiménez & Dudhia, 2018).

3.2. Impacts of Great Lakes Surface Temperature on Regional Atmosphere

3.2.1. Near-Surface Air Temperature and Evaporation

Next, we investigated the LST impacts across the entire GLR and over the GLHB (Figure 1). Although some atmospheric variables such as pressure were found to be largely unaffected by the different LST data sets, we did find changes in atmosphere and surface variables that influenced the water and energy budget over the GLR. These changes could potentially affect the convective environment and different types of precipitation, such as those associated with MCSs and IDCs. Figure 6 (top row) shows WRF_ELST simulated T2 and the difference in T2 simulated by WRF_ESLT and WRF_GLST. Both experiments captured the spatial variation in T2, but WRF_GLST simulated a warmer T2 than WRF_ELST, consistent with the evaluations against buoy stations (Figures 4 and 5). The magnitude of the warming in T2 was 2 times larger than the internal variability of T2 over most of the GLHB; therefore, we considered the impact of LST on T2 to be statistically significant at the 95% confidence level over these areas.

Figure 6 (bottom row) shows the evaporation calculated with latent heat flux from the WRF output and the difference in evaporation between WRF_ELST and WRF_GLST. Because lake surface was still cooler than the surrounding atmosphere throughout most of the months (June–August) studied here, there were very minor negative evaporation values (condensation) over the northern lakes, consistent with observations (Lenters, 2004; Lenters et al., 2013). The evaporation rates on the Great Lakes typically start increase in late fall and reach the maximum in early winter due to a large temperature difference between water and air (i.e., warm water and cold air), low relative humidity, and high wind speeds. In summer months, evaporation over land and the warmer southern/shallow lakes (e.g., Lake Erie) was larger than that over northern lakes. Compared to WRF_ELST, WRF_GLST simulated significant increased evaporation caused by more latent heat flux due to the warmer GLST, especially over the southern lakes. For example, over Lake Erie and Lake Ontario, the evaporation increased in WRF_GLST by almost 50% along the southern coast. Similar increases were also seen over the southern coast of Lake Michigan and Lake Huron, adding extra moisture to the atmosphere and providing a favorable condition for precipitation development.

3.2.2. Moisture

Figure 7 (top row) shows the IVT in June–August simulated by WRF_ELST, and the difference in IVT between WRF_GLST and WRF_ELST. The IVT represents the net moisture transported in and out of an atmospheric column. In summer, the warm moisture comes from the Southern Great Plains and is transported to the eastern GLR. With the warmer LST used in WRF_GLST, an anomalous cyclonic circulation formed over the majority of the GLR. This cyclonic circulation indicated different impacts on the moisture transport over the western GLR and eastern GLR. Over the western GLR (e.g., Iowa, Wisconsin, and Minnesota), WRF_GLST reduced the south-to-north moisture flux transport, which potentially decreased the chance of MCS-induced precipitation that propagates from the western United States. Over the southern and the eastern GLR, WRF_GLST intensified the warm moisture transport to the northeastern GLR, providing extra moisture for precipitation development.

Figure 7 (bottom row) shows the WRF_ELST simulated PWAT and the changes caused by the warmer LST from WRF_GLST. Averaged across the summer season there was only a minor impact on the PWAT. Looking at the 3 months individually, we found that the PWAT increased more significantly in June and August over the eastern GLR, namely Lake Michigan, the state of Michigan, Lake Huron, and Lake Erie. The PWAT was increased by 0.2–0.4 mm day^{-1} (statistically significant) over the majority of these lakes and central and southern Michigan State. The spatial pattern of increased PWAT was also consistent with the increases in evaporation, indicating that the increased evaporation caused by the warmer GLST may enhance moisture availability and transport, particularly to eastern GLR. The effect of these changes on precipitation patterns is discussed in Section 3.2.4.

3.2.3. Convective Environment

Figure 8 (top row) shows the MCAPE computed by lifting the air parcel with the maximum equivalent potential temperature simulated by WRF_ELST, and the difference in MCAPE between WRF_ELST and WRF_GLST. In both WRF_ELST and WRF_GLST, the MCAPEs were relatively large (up to 1,000 J kg^{-1}) over land (e.g., the southwestern GLR), which was beneficial for MCS development and maintaining their propagation from the

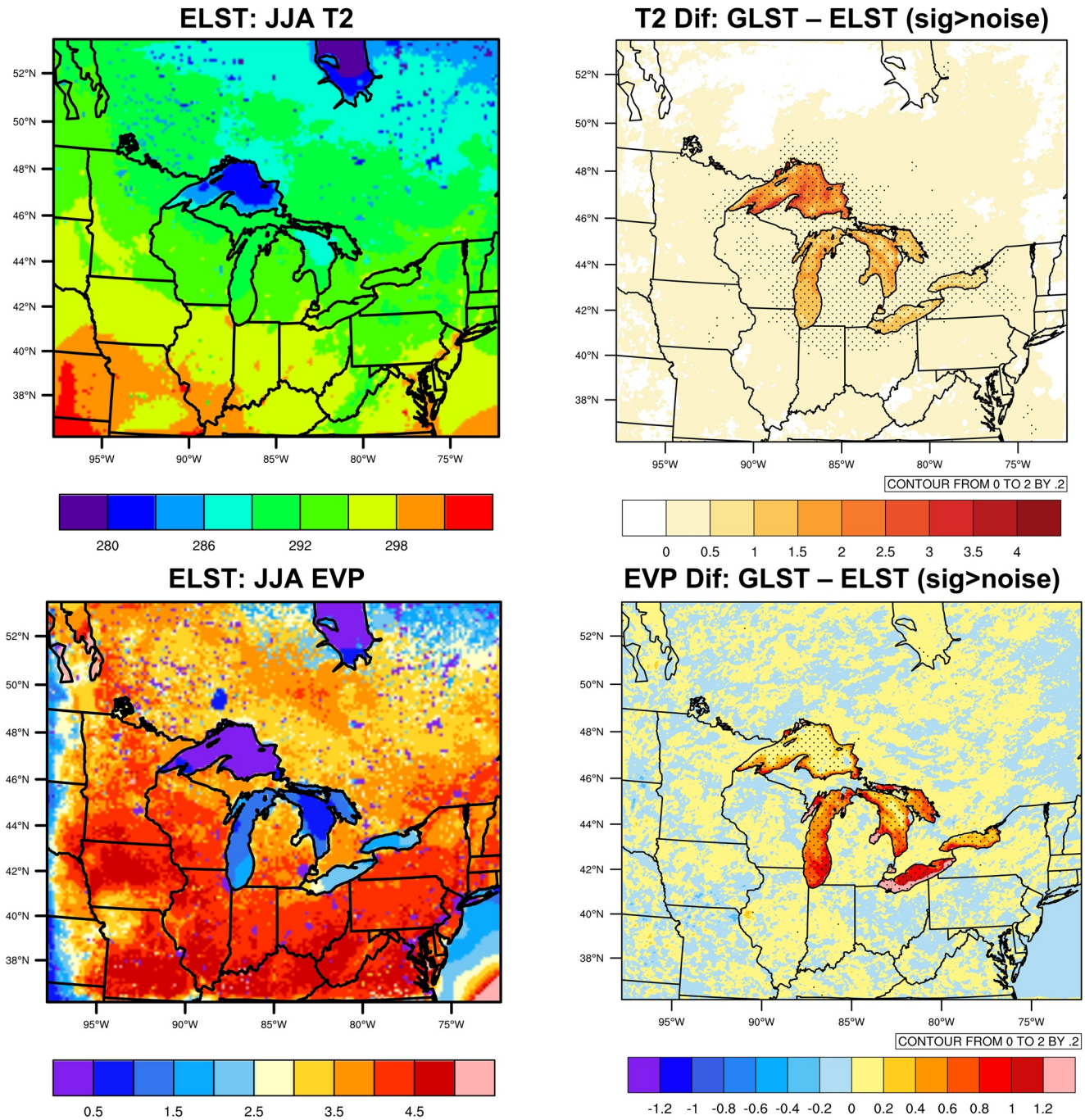

Figure 6. Left: WRF_ELST simulated 2-m air temperature (T2, °K) and evaporation (mm day^{-1}) derived from latent heat flux. Right: difference in T2 and evaporation between WRF_ELST and WRF_GLST (WRF_GLST minus WRF_ELST). All results are based on the ensemble mean from the 10 ensemble members in summer 2018. The stipples indicate that the differences are at least two times larger than the model internal variability.

western United States. The MCAPEs were smaller over the Great Lakes and the downstream over the northeastern GLR because stable conditions were created by the temperature difference between the lake (e.g., cooler) and the atmosphere (e.g., warmer).

With the warmer GLST used in the WRF_GLST simulations, the MCAPE was significantly larger, on the order of 40–60 J kg^{-1}, over the majority of the GLHB—especially over southern Lake Michigan, Lake Huron, Lake Erie,

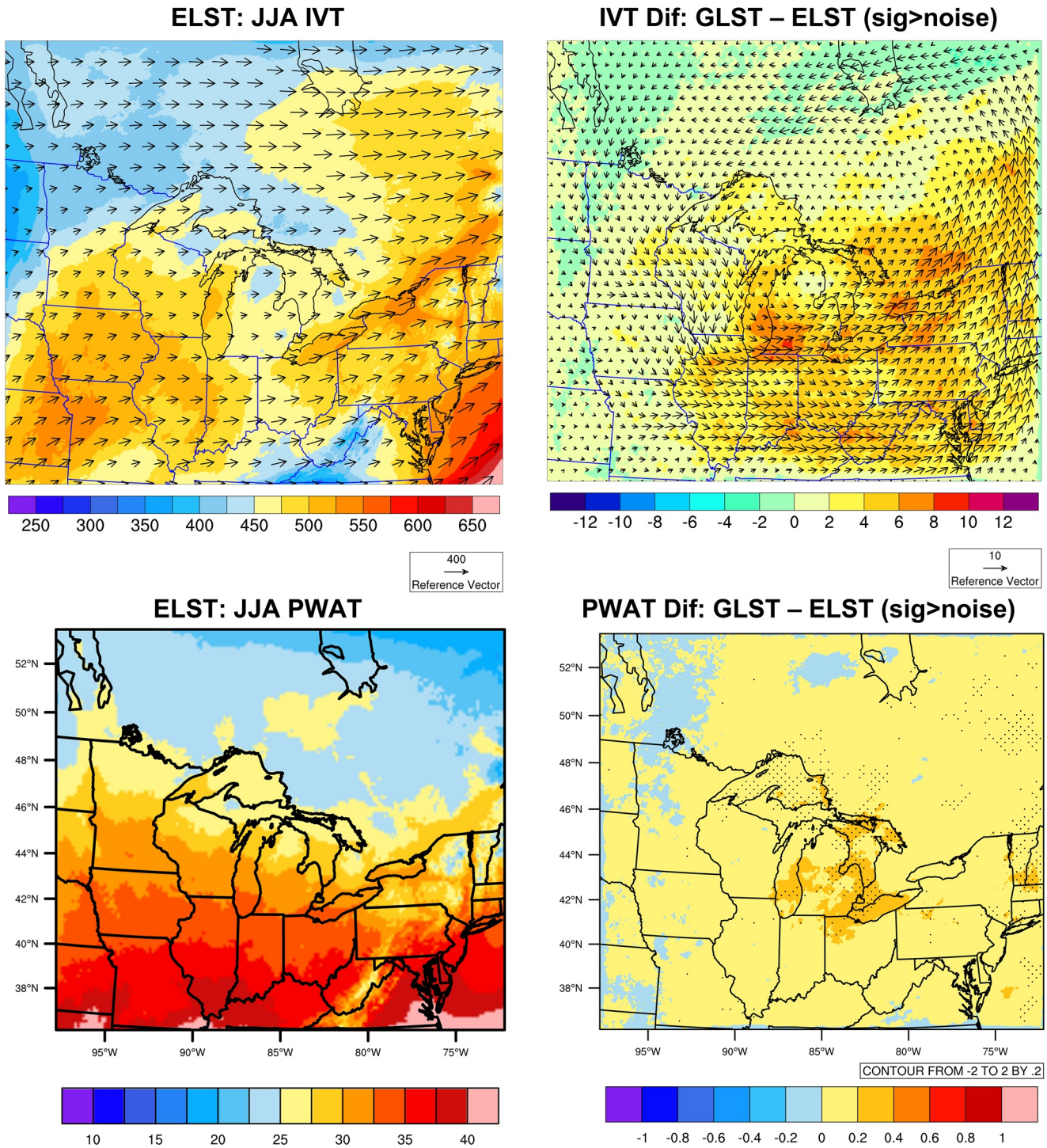

Figure 7. Left: WRF_ELST simulated integrated water vapor transport (IVT, kg m^{-1} s^{-1}) and precipitable water (PWAT, mm day^{-1}) derived from vertical profile of temperature, water vapor mixing ratio, and wind components. Right: difference in IVT and PWAT between WRF_ELST and WRF_GLST (WRF_GLST minus WRF_ELST). All results are based on the ensemble mean from the 10 ensemble members in summer 2018. The stipples indicate that the differences are at least two times larger than model internal variability.

and Lake Ontario. We also saw significantly reduced LCL height (Figure 8, bottom row), indicating less moisture deficit, over most of the lakes because more moisture was available due to the warmer GLST. The decrease in LCL height was on the order of 60–120 m across much of the GLHB. These results suggest that the difference in LST could potentially influence the GLR convective environment and change the thermodynamic instability of

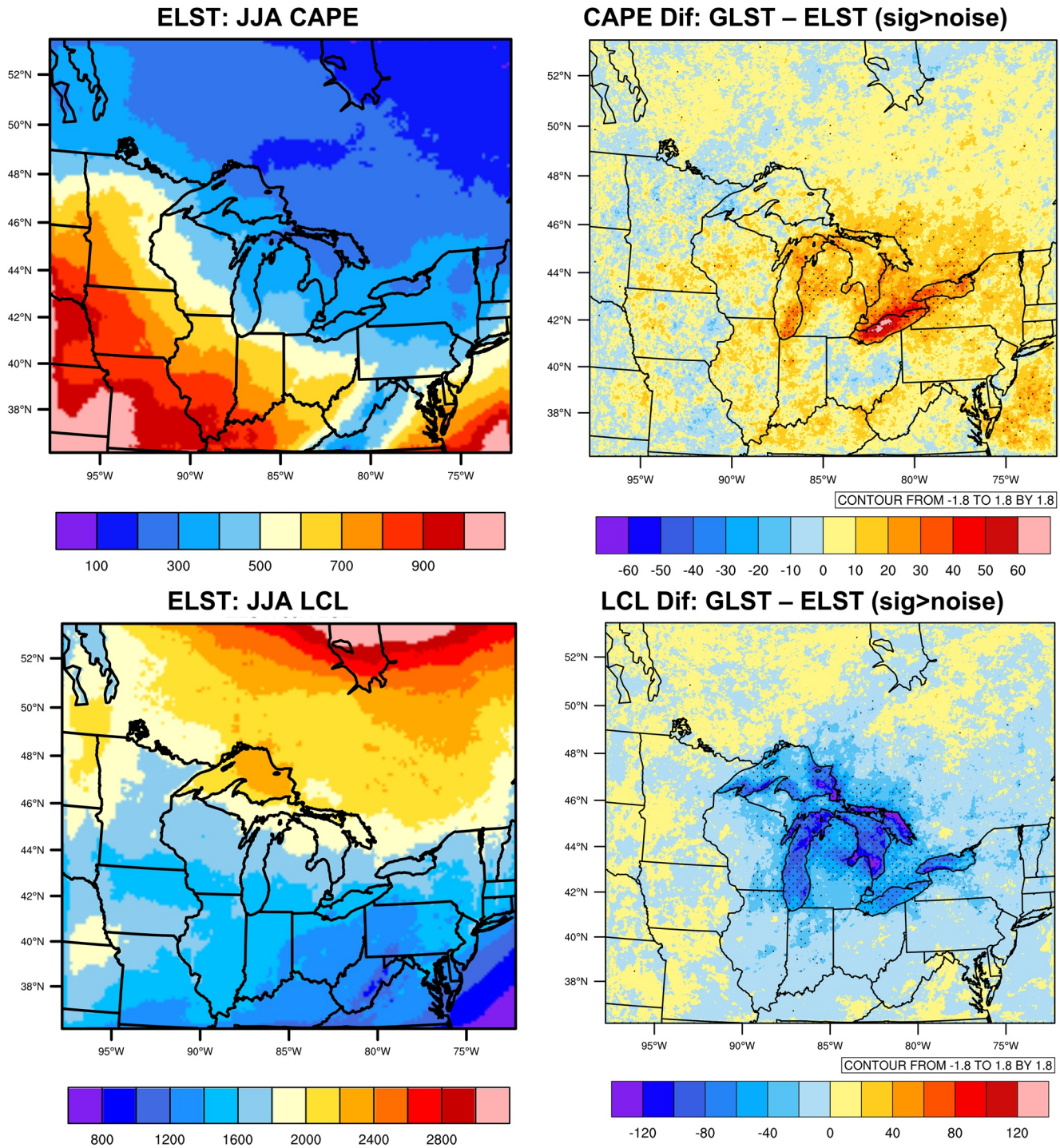

Figure 8. Left: WRF_ELST simulated maximum convective available potential energy (MCAPE, J kg^{-1}) and lifting condensation level (LCL, m). Right: difference in MCAPE and LCL between WRF_ELST and WRF_GLST (WRF_GLST minus WRF_ELST). All results are based on the ensemble mean from the 10 ensemble members in summer 2018. The stipples indicate that the differences are at least two times larger than model internal variability.

the atmosphere. These changes occurred because the warmer GLST used in WRF_GLST subsequently increased latent heating and available moisture, including the moisture evaporated from the lakes and transferred from the south (Figures 6 and 7). The added moisture made the atmosphere more convectively unstable, reducing the LCL height, and increasing MCAPE (Chen et al., 2020).

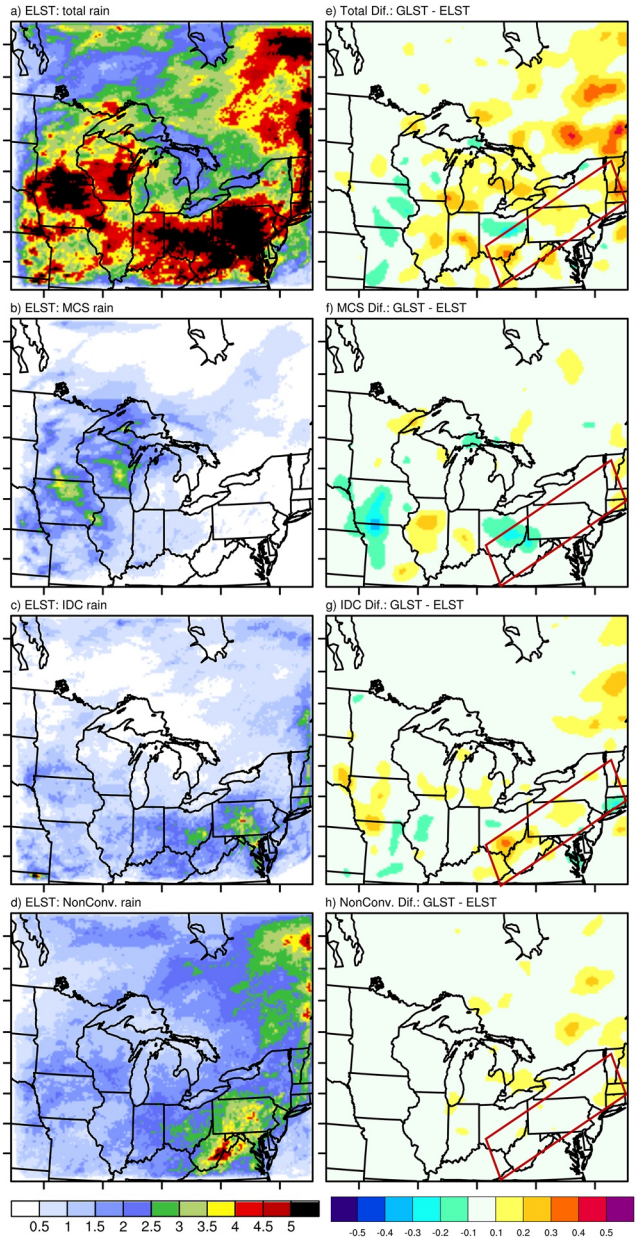

Figure 9. Top row: total precipitation amount. Second row: mesoscale convective system (MCS)-induced precipitation amount. Third row: isolated deep convection (IDC)-induced precipitation amount. Bottom row: nonconvective precipitation amount. Left: WRF_ELST produced precipitation. Right: the differences between WRF_ELST and WRF_GLST (WRF_GLST minus WRF_ELST); a 2-D Gaussian filter was applied to the original differences with a size of 321 × 321 km^2 and a standard deviation of 40 km. Data are from the 10 ensemble members in summer (June–August) 2018. The difference of precipitation is smaller than or similar to (location dependent) the model internal variability.

3.2.4. Precipitation

Finally, we examined the changes in precipitation caused by the differences in LST between ELST and GLST across the five lakes. Local moisture evaporated from the lakes played an important role in precipitation over the GLHB. In Figure 9, first we look at the total precipitation over the entire GLR. Overall, 3.3 mm day^{-1} of total precipitation was generated by WRF_ELST; WRF_GLST generated 0.06 mm day^{-1} (1.8%) more precipitation averaged across the entire GLR. There was substantial spatial variability in the change from WRF_ELST to WRF_GLST, but none of the changes were statistically significant.

Next, we looked at the convective precipitation including MCS- and IDC-induced events tracked by the FLEXTRKR algorithm, and the nonconvective precipitation derived by subtracting the MCS and IDC precipitation amount from the total precipitation amount. We found that the MCS-induced precipitation was concentrated upwind of the GLHB or on the western side of the GLR and was much smaller over lakes and downwind of the GLHB because of the stable conditions caused by the relatively cool LST. There was 0.7 mm day^{-1} (21.8% of the total precipitation) of MCS-induced precipitation generated in WRF_ELST. WRF_GLST showed a very small increase (0.4%) in MCS-induced rainfall averaged across the entire GLR. However, there were local differences in the amount of precipitation simulated by the two WRF experiments. For example, WRF_GLST reduced MCS precipitation over Iowa, northern Missouri, and Ohio, but increased it over northern Illinois and central Indiana, and the change can be up to 50% over certain locations. The decrease in MCS precipitation over the western side of the GLR could potentially be due to the reduction of south-to-north moisture flux transport over Minnesota all the way to Missouri (Figure 7, top right).

The IDC is a more localized storm type that can be generated by the local moisture evaporated from the Great Lakes and by the moisture transferred from the southwest of the GLR (Figure 7). Overall, WRF_ELST generated 0.9 mm day^{-1} of IDC-induced precipitation (27.5% of the total precipitation) averaged across the GLR, more than the amount of MCS precipitation. WRF_GLST increased the IDC precipitation by 3.3% averaged across the entire GLR, much more than the increase for the MCS. These increases occurred downstream of the GLHB or on the eastern side of Lake Erie and Lake Ontario, because extra moisture was available due to increased evaporation and moisture transport, as well as the increase (decrease) in MCAPE (LCL) over these regions (Figure 8).

The nonconvective precipitation was mainly from stratiform rain and likely caused by larger scale circulations such as jet streams and midlatitude cyclones (Knox et al., 2008). These circulations generate relatively small amounts of precipitation in western GLR and more precipitation in the northeastern United States. WRF_ELST generated 1.7 mm day^{-1} of nonconvective precipitation (50.7% of all precipitation) averaged across the GLR. WRF_GLST increased the nonconvective precipitation by 1.8% averaged across the entire GLR. These results demonstrated that a different LST could influence different types of precipitation, caused by local and nonlocal systems, over and beyond the Great Lakes.

We also calculated the diurnal cycles of total precipitation, MCS- and IDC-induced precipitation, as well as nonconvective precipitation averaged across the GLHB as well as a subregion downstream of the GLHB. Figure 10 compares the results of the twin experiments in summer 2018 from 10 ensemble members. Both

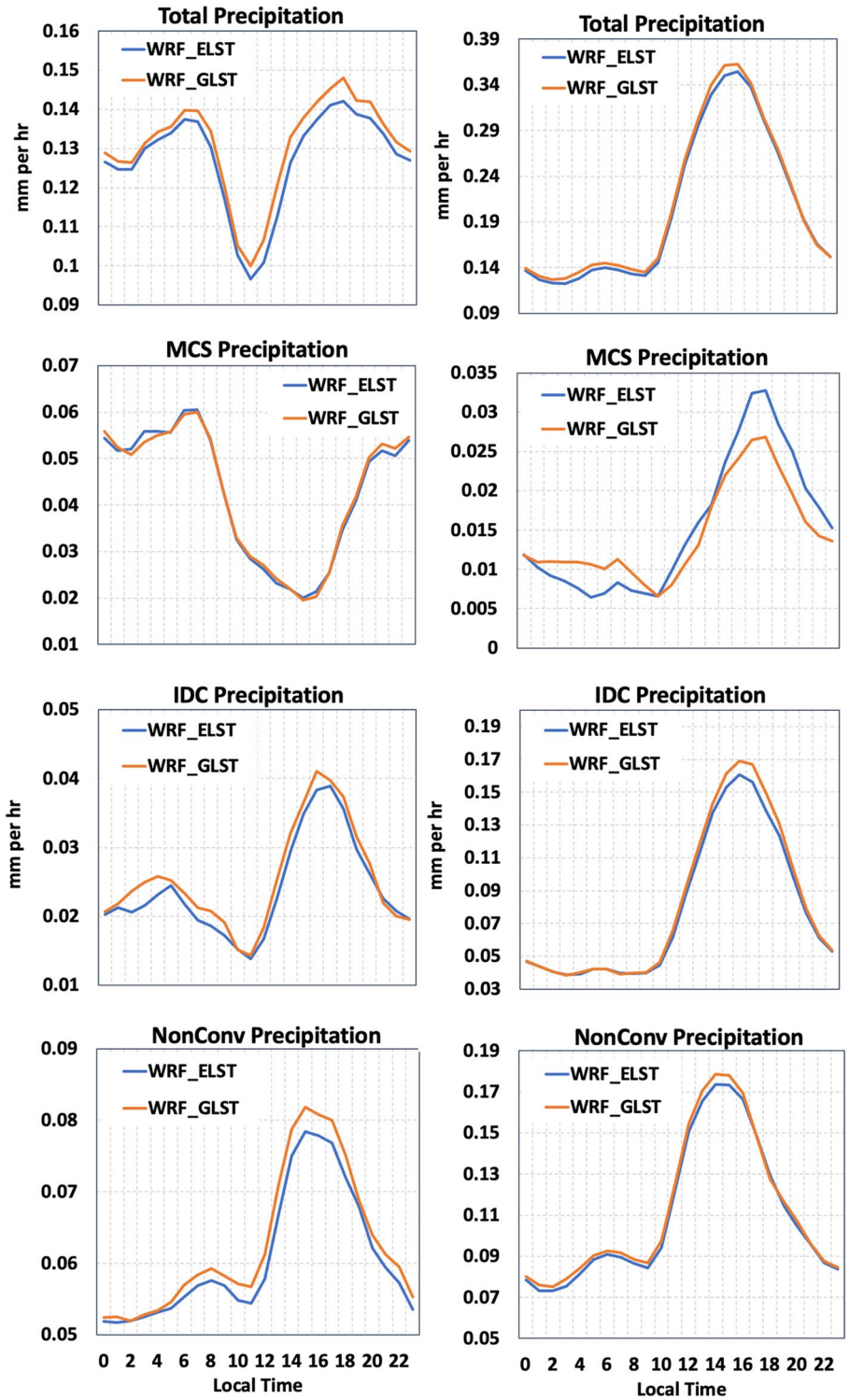

Figure 10. Diurnal patterns of subregional-averaged precipitation, including mesoscale convective system (MCS)-, isolated deep convection (IDC)-, and nonconvection-induced precipitation in summer 2018 from the 10 ensemble members in the twin experiments WRF_ELST and WRF_GLST. Left: Great Lakes Hydrological Basin (GLHB, blue in Figure 1)-averaged precipitation; right: downstream of GLHB, outlined by red boxes in Figure 9.

experiments showed that the maximum total precipitation would occur in early evening (~6 p.m. central time), and the smallest precipitation amount during midday (11 a.m.) over both GLHB and the downstream region, which is consistent with previous studies investigating the rainfall events in the warm season (Miner & Fritsch, 1997; Workoff et al., 2012).

The WRF_GLST generated more total precipitation than WRF_ELST at all times over GLHB, with the greatest increase during early afternoon (7%). When we decomposed the total precipitation amount into convective (including MCS- and IDC-induced) and nonconvective precipitation, we found that over GLHB, the peak during nighttime (3 a.m.) was mostly contributed by MCS-induced precipitation, while the peak in the late afternoon (4–6 p.m.) was contributed by IDC-induced and nonconvective precipitation. This is consistent with previous studies, which indicted that IDC precipitation peaks in the late afternoon in summer, reflecting the impact of local instability driven by the solar forcing on IDC development (Li et al., 2021). The diurnal peaks for MCS events, on the other hand, vary across different regions of the United States. For example, over downstream GLHB, the peak of MCS-induced precipitation is in the early evening (5–6 p.m.), because in summer they are usually initiated over the east of the Rocky Mountains (Front Range) and west of Kansas due to the strong diurnal heating over the Rocky Mountains in the local afternoon. With their subsequent eastward propagation into the GLR, the diurnal peaks of MCS occur in the nocturnal hours over the central and eastern United States (Feng et al., 2019), consistent with our finding.

While the MCS-induced precipitation did not change much over the GLHB, it is decreased over downstream of GLHB in the afternoon to early evening. The IDC-induced precipitation and nonconvective precipitation were both increased in WRF_GLST by up to 15.8% (midnight, for IDC events) and 6.2% (midday, for nonconvective events), respectively, over both GLHB and downstream of GLHB. This result suggests that even though the LST is only different over the Great Lakes, the impacts of such a difference on the atmosphere can extend to a larger scale and influence not only the relatively small-scale convection processes but also nonconvective processes that are associated with synoptic scale forcing. In this case, because of the intensification to the moisture transport (from south to northeast) due to the warmer GLST, the nonconvective precipitation was enhanced.

3.3. Internal Variability and Interannual Variability

In this section, we investigate how important the internal and interannual variabilities are when comparing with the impacts from the difference in LST. First, we conducted the same analysis as for the 10 ensemble members using the 2014–2020 summer results to examine the changes in T2, evaporation, IVT, and PWAT, as well as different types of precipitation due to the warmer GLST used in WRF_GLST compared with WRF_ELST. To test the robustness of the difference in these variables caused by the LST difference, Student's *t* test for the hourly time series of the 7-year averages was conducted over each grid cell.

In general, we saw similar impacts of the LST difference in the 7-year simulations to the 10-ensemble simulation in 2018. For example, both T2 and evaporation were increased significantly over the GLHB. There were also anomalous cyclonic circulations generated by the warmer GLST over the GLR, which intensified the moisture flux transport and increased the IDC-induced precipitation over the eastern GLR. In terms of the diurnal pattern of precipitation, while the individual years generated different amount of precipitation (e.g., 2015 showed the lowest precipitation and 2017 showed the highest precipitation amount), WRF_GLST always generated more total precipitation than WRF_ELST in each single year. These results indicate that the response of the WRF simulations to a different LST is always in the same sign, although they could be at different magnitudes, depending on the atmospheric conditions in a given year.

Next, we compared the interannual variability with the internal variability, demonstrated by the 7-year simulations and 10 ensemble simulations in 2018, respectively. Figure 11 shows the mean, maximum and minimum of the 7-year simulation, and 10 individual ensemble members from the WRF_GLST for diurnal pattern of precipitation in June–August, daily time series of T2, and evaporation, averaged across the GLHB. Note that calculating the daily and basin-wide mean of each variable significantly reduces both their internal and interannual variabilities compared with the hourly data over individual grid cells, because the averaging smooths out the small-scale variabilities.

We see that for all variables, the internal variability (Figure 11, blue lines) is always smaller than the interannual variability (red shading, bounded by maximum and minimum at each time point). This is because the 10 ensemble

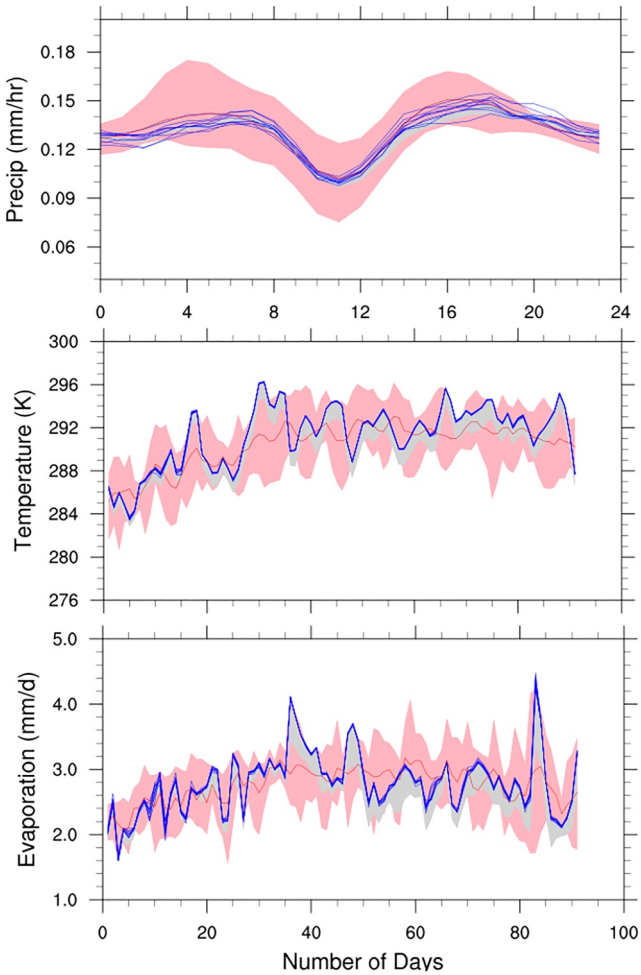

Figure 11. Internal variability (spread shown by the blue lines) and interannual variability (red shading bounded by minimum and maximum at each time point) of diurnal precipitation, daily T2, evaporation, and MCAPE. Red line: 7-year average. Gray shading: difference in each variable between WRF_ELST and WRF_GLST. All the data are from the experiment WRF_GLST, except the difference in each variable, which is shown by WRF_ELST and WRF_GLST using the 10-ensemble mean in 2018.

members are from the same year and only differ in their initial conditions; the seven-summer simulations could be influenced by atmospheric oscillations at different time scales, including the very strong El Niño year in 2015–2016 and moderate La Niña year in 2020. The differences between WRF_ELST and WRF_GLST based on 2018 results (gray shading) for all the variables were mostly larger than the internal variabilities (except for precipitation) but smaller than the interannual variability. This implies that for this study the lateral boundary conditions were mostly dominant over the initial conditions and the lower lake boundary conditions, and the impact of the lower lake boundary is larger than the impact of initial conditions for most of the variables assessed here. The influence of LST difference in our study was relatively small because both LST data sets do a reasonably good job of reproducing LST observations overall. In addition, the impacts presented in this study are based on climatology rather than individual events. The impact (gray shading) could be much larger when using a LST that has a greater discrepancy with observations (e.g., Spero et al., 2016) and when examining the impacts of LST differential at an event-scale.

4. Summary and Discussion

This study conducted a set of twin experiments using the latest version of WRF model version 4.2.2 at a spatial resolution of 4 km forced by the ERA5 reanalysis data to demonstrate the impact of using a different LST on the regional climate over the GLR. These experiments used the same model setup, except that they were driven by two different LST data sets as the lower atmospheric boundary condition over lake areas.

Overall, this study found that using different LST data sets as lower boundary conditions in regional climate modeling can influence not only the local atmosphere but also the nonlocal atmospheric conditions, which shows how important it is for LST to be accurate over the Great Lakes. For example, forced by warmer GLST, WRF produced air temperatures over Lake Superior and Lake Erie were significantly warmer (by 1.93°C and 0.97°C, respectively). The latent heat flux over the lakes was also significantly increased, causing more evaporations over the GLHB (0.23 and 1.1 mm day^{-1} over Lake Superior and Lake Erie) and providing extra moisture for precipitation development. The moisture flux transport and the convective environment were also intensified downwind of the GLHB, providing conditions that were favorable for the formation of local precipitation on the eastern side of Great Lakes. The impact of the warmer GLST on precipitation, however, could expand beyond the GLHB due to the cyclonic circulation for moisture flux transport, which can weaken the potential of precipitation over the western GLR, but strengthen the precipitation potential over the eastern GLR. Therefore, the MCS-induced precipitation was lower over the western GLR, where it mostly occurs, while the IDC-induced and nonconvective precipitation was higher downwind of the GLR. These impacts indicate that use of inaccurate LST data can lead to biased evaporation and precipitation over the lake surface and near-coastal land surface, which can affect both short- and long-term forecasting of lake levels as well as convective precipitation near the lakes.

The LST difference in our twin experiments was relatively small compared with interannual variability of the LST, so not surprisingly, their impacts were also not large because the two LST data sets (ELST and GLST) were both from observations rather than from sensitivity experiments in which two scenarios can be exaggeratedly different (e.g., Spero et al., 2016). The impact is also relatively small because we focus on quantifying the climate impacts using summer average. We expect that such impacts could be much larger if the LST difference were larger than the difference studied here (around ~1.4°C on average), which could be the case for many GCMs that use skin temperature as the LST over the Great Lakes (e.g., CESM version 2.0, used by the Coupled Model

Intercomparison Project phase 6). Such impacts could be also larger if we examine individual events. While the basin-averaged precipitation change is minor, the precipitation change in each single event can be substantial in both magnitude and spatial patterns. On the other hand, if we put this LST difference (between ELST and GLST) in the context of climate change, it is equivalent to the LST warming under Representative Concentration Pathway 4.5 by midcentury or even late-century (1–3°K). Such warming can cause 5%–10% increase for precipitation in future over the GLHB, based on a two-way coupled climate model with a 3-D lake model by Xue et al. (2022).

Although the approach used by this study (e.g., collecting and/or calibrating observations for more accurate LST) may have been sufficient for historical simulations because high-resolution observed water temperature data were available, it is not possible for RCM-based future projections. Instead, water temperatures from the nearest ocean SST in GCMs were often used, which likely caused significant bias in the modeled climate. For example, when using default CESM's SST data as lower boundary conditions in WRF, the LSTs are more than 14°K warmer than Community Land Model-Lake prediction over the southern and eastern Great Lakes and are 5°K cooler over the western Lake Superior (Spero et al., 2016). Therefore, in RCMs, the atmosphere model needs to be coupled with a realistic model of the lake that can fully resolve the lake dynamics and physics and the atmosphere–lake feedback (Sharma et al., 2018; Xue et al., 2017) in order to properly represent the regional climate across the GLR as demonstrated here based on the effect of LST.

Data Availability Statement

Data sets used in this study may be downloaded at the following URL: ERA5: https://cds.climate.copernicus.eu/cdsapp#!/dataset/reanalysis-era5-pressure-levels?tab=form. NDBC: https://www.ndbc.noaa.gov/. GLSEA satellite-derived LST: https://coastwatch.glerl.noaa.gov/glsea/doc/.

Acknowledgments
This study is supported by COMPASS-GLM, a multi-institutional project supported by the U.S. Department of Energy, Office of Science, Office of Biological and Environmental Research as part of the Regional and Global Modeling and Analysis (RGMA) program, Multi-sector Dynamics Modeling (MSD) program, and Earth System Model Development (ESMD) program. This study is also Contribution No. 92 of the Great Lakes Research Center at Michigan Technological University. Computational resources are provided by the DOE-supported National Energy Research Scientific Computing Center and Argonne Leadership Computing Facility. All the calculations are done using the NCAR Command Language (version 6.6.2; software), 2019, Boulder, CO: UCAR/NCAR/CISL/TDD, http://dx.doi.org/10.5065/D6WD3XH5. The Pacific Northwest National Laboratory is operated for DOE by Battelle Memorial Institute under contract DE-AC05-76RL01830.

References

Austin, J. A., & Colman, S. M. (2007). Lake Superior summer water temperatures are increasing more rapidly than regional air temperatures: A positive ice-albedo feedback. *Geophysical Research Letters*, *34*, L06604. https://doi.org/10.1029/2006GL029021

Bell, B., Hersbach, H., Berrisford, P., Dahlgren, P., Horányi, A., Sabater, M., et al. (2020). *ERA5 hourly data on pressure levels from 1950 to 1978 (preliminary version)*. Copenhagen: Copernicus Climate Change Service (C3S) Climate Data Store (CDS). Retrieved from https://cds.climate.copernicus-climate.eu/cdsapp#!/dataset/reanalysis-era5-pressure-levels-preliminary-back-extension?tab=overview

Chang, W., Stein, M. L., Wang, J., Kotamarthi, V. R., & Moyer, E. J. (2016). Changes in spatiotemporal precipitation patterns in changing climate conditions. *Journal of Climate*, *29*(23), 8355–8376. https://doi.org/10.1175/JCLI-D-15-0844.1

Chen, F., & Dudhia, J. (2001). Coupling an advanced land surface–hydrology model with the Penn State–NCAR MM5 modeling system. Part I: Model implementation and sensitivity. *Monthly Weather Review*, *129*, 569–585. https://doi.org/10.1175/1520-0493(2001)129<0569:CAALSH>2.0.CO;2

Chen, J., Dai, A., Zhang, Y., & Rasmussen, K. L. (2020). Changes in convective available potential energy and convective inhibition under global warming. *Journal of Climate*, *33*(6), 2025–2050. https://doi.org/10.1175/JCLI-D-19-0461.1

Christensen, J. H., Carter, T. R., Rummukainen, M., & Amanatidis, G. (2007). Evaluating the performance and utility of regional climate models: The PRUDENCE project. *Climatic Change*, *81*, 1–6. https://doi.org/10.1007/s10584-006-9211-6

Delaney, F., & Milner, G. (2019). *The state of climate modeling in the Great Lakes Basin—A synthesis in support of a workshop held on June 27, 2019 in Ann Arbor, MI*. Toronto, Canada: Ontario Climate Consortium.

Donlon, C. J., Martin, M., Stark, J., Roberts-Jones, J., Fiedler, E., & Wimmer, W. (2012). The operational sea surface temperature and sea ice analysis (OSTIA) system. *Remote Sensing of Environment*, *116*, 140–158. https://doi.org/10.1016/j.rse.2010.10.017

EPA (U.S. Environmental Protection Agency). (2020). *Physical features of the Great Lakes*. Retrieved from https://www.epa.gov/greatlakes/physical-features-great-lakes

Feng, Z., Houze, R. A., Leung, L. R., Song, F., Hardin, J. C., Wang, J., et al. (2019). Spatiotemporal characteristics and large-scale environments of mesoscale convective systems east of the Rocky Mountains. *Journal of Climate*, *32*(21), 7303–7328. https://doi.org/10.1175/JCLI-D-19-0137.1

Feng, Z., Leung, L. R., Hagos, S., Houze, R. A., Burleyson, C. D., & Balaguru, K. (2016). More frequent intense and long-lived storms dominate the springtime trend in central US rainfall. *Nature Communications*, *7*(1), 1–8. https://doi.org/10.1038/ncomms13429

Feng, Z., Leung, L. R., Houze, R. A., Hagos, S., Hardin, J., Yang, Q., et al. (2018). Structure and evolution of mesoscale convective systems: Sensitivity to cloud microphysics in convection-permitting simulations over the United States. *Journal of Advances in Modeling Earth Systems*, *10*, 1470–1494. https://doi.org/10.1029/2018MS001305

Gula, J., & Peltier, W. R. (2012). Dynamical downscaling over the Great Lakes Basin of North America using the WRF regional climate model: The impact of the Great Lakes system on regional greenhouse warming. *Journal of Climate*, *25*(21), 7723–7742. https://doi.org/10.1175/JCLI-D-11-00388.1

Harris, L., & Kotamarthi, V. R. (2005). The characteristics of the Chicago lake breeze and its effects on trace particle transport: Results from an episodic event simulation. *Journal of Applied Meteorology*, *44*(11), 1637–1654. https://doi.org/10.1175/jam2301.1

Hong, S. Y., & Lim, J. J. (2006). The WRF single-moment 6-class microphysics scheme (WSM6). *Journal of the Korean Meteorological Society*, *42*, 129–151.

Hu, H. C., Leung, L. R., & Feng, Z. (2020). Observed warm-season characteristics of MCS and non-MCS rainfall and their recent changes in the central United States. *Geophysical Research Letters*, *47*, e2019GL086783. https://doi.org/10.1029/2019GL086783

Iacono, M. J., Delamere, J. S., Mlawer, E. J., Shephard, M. W., Clough, S. A., & Collins, W. D. (2008). Radiative forcing by long-lived greenhouse gases: Calculations with the AER radiative transfer models. *Journal of Geophysical Research*, *113*, D13103. https://doi.org/10.1029/2008JD009944

Jiménez, P. A., & Dudhia, J. (2018). On the need to modify the sea surface roughness formulation over shallow waters. *Journal of Applied Meteorology and Climatology*, *57*(5), 1101–1110. https://doi.org/10.1175/JAMC-D-17-0137.1

Jiménez, P. A., Dudhia, J., González-Rouco, J. F., Navarro, J., Montávez, J. P., & García-Bustamante, E. (2012). A revised scheme for the WRF surface layer formulation. *Monthly Weather Review*, *140*(3), 898–918.

Knox, J. A., Lacke, M. C., Frye, J. D., Stewart, A. E., Durkee, J. D., Fuhrmann, C. M., & Dillingham, S. M. (2008). *Non-convective high wind events: A climatology for the Great Lakes Region*. Paper presented at 24th Conference on Severe Local Storms, American Meteorological Society, Savannah, GA.

Kunkel, K. E., Easterling, D. R., Kristvich, D. A. R., Gleason, B., Stoecker, L., & Smith, R. (2012). Meteorological causes of the secular variations in observed extreme precipitation events for the conterminous United States. *Journal of Hydrometeorology*, *13*(3), 1131–1141. https://doi.org/10.1175/JHM-D-11-0108.1

Kunkel, K. E., Easterling, D. R., Redmond, K., & Hubbard, K. (2003). Temporal variations of extreme precipitation events in the United States: 1895–2000. *Geophysical Research Letters*, *30*(17), 1900. https://doi.org/10.1029/2003GL018052

Lahmers, T. M., Castro, C. L., & Hazenberg, P. (2020). Effects of lateral flow on the convective environment in a coupled hydrometeorological modeling system in a semiarid environment. *Journal of Hydrometeorology*, *21*(4), 615–642. https://doi.org/10.1175/JHM-D-19-0100.1

Laird, N. F., & Kristovich, D. A. R. (2002). Variations of sensible and latent heat fluxes from a Great Lakes Buoy and associated synoptic weather patterns. *Journal of Hydrometeorology*, *3*(1), 3–12. https://doi.org/10.1175/1525-7541(2002)003<0003:VOSALH>2.0.CO;2

Lavers, D. A., & Villarini, G. (2013). Atmospheric rivers and flooding over the central United States. *Journal of Climate*, *26*, 7829–7836. https://doi.org/10.1175/JCLI-D-13-00212.1

Lenters, J. D. (2004). Trends in the Lake Superior water budget since 1948: A weakening seasonal cycle. *Journal of Great Lakes Research*, *30*(Suppl. 1), 20–40. https://doi.org/10.1016/s0380-1330(04)70375-5

Lenters, J. D., Anderton, J. B., Blanken, P., Spence, C., & Suyker, A. E. (2013). Assessing the impacts of climate variability and change on Great Lakes evaporation. In D. Brown, D. Bidwell, & L. Briley (Eds.), *2011 project reports*. Retrieved from the Great Lakes Integrated Sciences and Assessments (GLISA) Center http://glisaclimate.org/media/GLISA_Lake_Evaporation.pdf

Li, J., Feng, Z., Qian, Y., & Leung, L. R. (2021). A high-resolution unified observational data product of mesoscale convective systems and isolated deep convection in the United States for 2004–2017. *Earth System Science Data*, *13*(2), 827–856. https://doi.org/10.5194/essd-13-827-2021

Liu, C., Ikeda, K., Rasmussen, R., Barlage, M., Newman, A. J., Prein, A. F., et al. (2017). Continental-scale convection-permitting modeling of the current and future climate of North America. *Climate Dynamics*, *49*(1), 71–95. https://doi.org/10.1007/s00382-016-3327-9

Liu, W. T., Katsaros, K. B., & Businger, J. A. (1979). Bulk parameterization of air–sea exchanges of heat and water vapor including the molecular constraints at the interface. *Journal of the Atmospheric Sciences*, *36*(9), 1722–1734. https://doi.org/10.1175/1520-0469(1979)036<1722:BPOASE>2.0.CO;2

Mallard, M. S., Nolte, C. G., Spero, T. L., Bullock, O. R., Alapaty, K., Herwehe, J. A., et al. (2015). Technical challenges and solutions in representing lakes when using WRF in downscaling applications. *Geoscientific Model Development*, *8*(4), 1085. https://doi.org/10.5194/gmd-8-1085-2015

Mearns, L. O., Gutowski, W., Jones, R., Leung, R., McGinnis, S., Nunes, A., & Qian, Y. (2009). A regional climate change assessment program for North America. *Eos Transactions*, *90*, 311. https://doi.org/10.1029/2009EO360002

Miner, T. J., & Fritsch, J. M. (1997). Lake-effect rain events. *Monthly Weather Review*, *125*(12), 3231–3248. https://doi.org/10.1175/1520-0493(1997)125<3231:LERE>2.0.CO;2

Mironov, D., Terzhevik, A., Beyrich, F., & Heise, E. (2004). A lake model for use in numerical weather prediction systems. In J. Cote (Ed.), *Research activities in atmospheric and oceanic modelling* (Report No. 34, April 2004, WMO/TD-No. 1220, 4.23–4.24). Retrieved from http://www.cmc.ec.gc.ca/rpn/wgne/2004/individual-articles/04MironovDmitriiMTBHWMOBlueBook04.pdf

Noh, Y., Cheon, W. G., Hong, S. Y., & Raasch, S. (2003). Improvement of the K-profile model for the planetary boundary layer based on large eddy simulation data. *Boundary-Layer Meteorology*, *107*, 401–427. https://doi.org/10.1023/a:1022146015946

Notaro, M., Holman, K., Zarrin, A., Fluck, E., Vavrus, S., & Bennington, V. (2013). Influence of the Laurentian Great Lakes on regional climate. *Journal of Climate*, *26*(3), 789–804. https://doi.org/10.1175/JCLI-D-12-00140.1

Notaro, M., Zhong, Y., Xue, P., Peters-Lidard, C., Cruz, C., Kemp, E., et al. (2021). Cold season performance of the NU-WRF regional climate model in the Great Lakes Region. *Journal of Hydrometeorology*, *22*(9), 2423–2454. https://doi.org/10.1175/JHM-D-21-0025.1

Prein, A. F., Liu, C., Ikeda, K., Bullock, R., Rasmussen, R. M., Holland, G. J., & Clark, M. (2020). Simulating North American mesoscale convective systems with a convection-permitting climate model. *Climate Dynamics*, *55*(1), 95–110. https://doi.org/10.1007/s00382-017-3993-2

Santanello, J. A., Jr., Dirmeyer, P. A., Ferguson, C. R., Findell, K. L., Tawfik, A. B., Berg, A., et al. (2018). Land–atmosphere interactions: The LoCo perspective. *Bulletin of the American Meteorological Society*, *99*(6), 1253–1272. https://doi.org/10.1175/BAMS-D-17-0001.1

Schulkowski, S. (2020). *Lake-effect dry periods in the Great Lakes Region during the late spring and early summer months* (master's thesis). Retrieved from Digital Commons @ ESF Syracuse, NY: State University of New York College of Environmental Science and Forestry. https://digitalcommons.esf.edu/etds/186

Schumacher, R. S., & Rasmussen, K. L. (2020). The formation, character and changing nature of mesoscale convective systems. *Nature Reviews Earth & Environment*, *1*(6), 300–314. https://doi.org/10.1038/s43017-020-0057-7

Schwab, D. J., Leshkevich, G. A., & Muhr, G. C. (1992). Satellite measurements of surface water temperature in the Great Lakes: Great Lakes Coast Watch. *Journal of Great Lakes Research*, *18*(2), 247–258. https://doi.org/10.1016/s0380-1330(92)71292-1

Scinocca, J. F., Kharin, V. V., Jiao, Y., Qian, M. W., Lazare, M., Solheim, L., et al. (2016). Coordinated global and regional climate modeling. *Journal of Climate*, *29*(1), 17–35. https://doi.org/10.1175/JCLI-D-15-0161.1

Scott, R. W., & Huff, F. A. (1996). Impacts of the Great Lakes on regional climate conditions. *Journal of Great Lakes Research*, *22*(4), 845–863. https://doi.org/10.1016/s0380-1330(96)71006-7

Sharma, A., Hamlet, A. F., Fernando, H. J. S., Catlett, C. E., Horton, D. E., Kotamarthi, V. R., et al. (2018). The need for an integrated land–lake–atmosphere modeling system, exemplified by North America's Great Lakes Region. *Earth's Future*, *6*, 1366–1379. https://doi.org/10.1029/2018EF000870

Shi, Q., & Xue, P. (2019). Impact of lake surface temperature variations on lake effect snow over the Great Lakes Region. *Journal of Geophysical Research: Atmospheres*, *124*, 12553–12567. https://doi.org/10.1029/2019JD031261

Simmons, A., Hersbach, H., Muñoz-Sabater, J., Nicolas, J., Vamborg, F., Berrisford, P., et al. (2021). *Low frequency variability and trends in surface air temperature and humidity from ERA5 and other datasets*. Reading: European Centre for Medium-Range Weather Forecasts. https://doi.org/10.21957/ly5vbtbfd

Skamarock, W. C., & Klemp, J. B. (2008). A time-split non-hydrostatic atmospheric model for weather research and forecasting applications. *Journal of Computational Physics*, *227*, 3465–3485. https://doi.org/10.1016/j.jcp.2007.01.037

Spero, T. L., Nolte, C. G., Bowden, J. H., Mallard, M. S., & Herwehe, J. A. (2016). The impact of incongruous lake temperatures on regional climate extremes downscaled from the CMIP5 archive using the WRF model. *Journal of Climate*, *29*(2), 839–853. https://doi.org/10.1175/JCLI-D-15-0233.1

Sun, L., Liang, X. Z., & Xia, M. (2020). Developing the coupled CWRF-FVCOM modeling system to understand and predict atmosphere–watershed interactions over the Great Lakes Region. *Journal of Advances in Modeling Earth Systems*, *12*, e2020MS002319. https://doi.org/10.1029/2020MS002319

Thompson, G., Field, P. R., Rasmussen, R. M., & Hall, W. D. (2008). Explicit forecasts of winter precipitation using an improved bulk microphysics scheme. Part II: Implementation of a new snow parameterization. *Monthly Weather Review*, *136*(12), 5095–5115. https://doi.org/10.1175/2008mwr2387.1

Thompson, G., Rasmussen, R. M., & Manning, K. (2004). Explicit forecasts of winter precipitation using an improved bulk microphysics scheme. Part I: Description and sensitivity analysis. *Monthly Weather Review*, *132*, 519–542. https://doi.org/10.1175/1520-0493(2004)132<0519:EFOWPU>2.0.CO;2

Wang, J., Bessac, J., Kotamarthi, R., Constantinescu, E., & Drewniak, B. (2018). Internal variability of a dynamically downscaled climate over North America. *Climate Dynamics*, *50*(11), 4539–4559. https://doi.org/10.1007/s00382-017-3889-1

Wang, J., & Kotamarthi, V. R. (2015). High-resolution dynamically downscaled projections of precipitation in the mid and late 21st century over North America. *Earth's Future*, *3*, 268–288. https://doi.org/10.1002/2015EF000304

Workoff, T. E., Kristovich, D. A., Laird, N. F., LaPlante, R., & Leins, D. (2012). Influence of the Lake Erie overlake boundary layer on deep convective storm evolution. *Weather and Forecasting*, *27*(5), 1279–1289. https://doi.org/10.1175/WAF-D-11-00076.1

Xiao, C., Lofgren, B. M., Wang, J., & Chu, P. Y. (2018). *A dynamical downscaling projection of future climate change in the Laurentian Great Lakes Region using a coupled air-lake model*. https://doi.org/10.20944/preprints201807.0468.v1

Xue, P., Pal, J. S., Ye, X., Lenters, J. D., Huang, C., & Chu, P. Y. (2017). Improving the simulation of large lakes in regional climate modeling: Two-way lake–atmosphere coupling with a 3D hydrodynamic model of the Great Lakes. *Journal of Climate*, *30*(5), 1605–1627. https://doi.org/10.1175/JCLI-D-16-0225.1

Xue, P., Ye, X., Pal, J. S., Chu, P. Y., Kayastha, M. B., & Huang, C. (2022). Climate projections over the Great Lakes Region: Using two-way coupling of a regional climate model with a 3-D lake model. *Geoscientific Model Development Discussions*, 1–37.

Zobel, Z., Wang, J., Wuebbles, D. J., & Kotamarthi, V. R. (2018). Analyses for high-resolution projections through the end of the 21st century for precipitation extremes over the United States. *Earth's Future*, *6*, 1471–1490. https://doi.org/10.1029/2018EF000956